



A new bounded kinematic controller for operational space motion of manipulators[☆]

Javier Moreno–Valenzuela^{a,*}, Carlos Torres–Torres^b

^a Instituto Politécnico Nacional–CITEDI, Ave. del Parque 1310, Mesa de Otay, Tijuana, B.C. 22510, Mexico

^b Sección de Estudios de Posgrado e Investigación–ESIME–IPN, Zacatenco, Distrito Federal 07738, Mexico

ARTICLE INFO

Article history:

Received 29 May 2009

Received in revised form 11 August 2010

Available online 15 September 2010

Kinematic controller
Bounded acceleration
Motion control
Operational space
Direct-drive robot

ABSTRACT

In this paper, a new operational space controller is introduced. The new scheme is based on a primary loop of joint velocity control and a secondary loop of kinematic control. The use of saturation functions in the kinematic controller allows producing on–line bounded acceleration commands, which has the advantage of preventing possible actuator damage. Sufficient conditions for the uniform asymptotic stability of this control system are provided. As additional contribution, experimental results carried on a two degrees-of-freedom direct-drive arm are shown.

© 2010 Elsevier Ltd. All rights reserved.

1. Introduction

Robot manipulator desired motions are typically specified in terms of trajectories of the end–effector posture in operational space (Canudas et al., 1996; Sciavicco and Siciliano, 2000). In order to execute the specified task, the inverse kinematics mapping can be used to translate from desired operational space trajectories to desired joint space trajectories. However, the computing of the inverse kinematics map can be a hard work for robots with many degrees of freedom.

In the pioneering work of resolved-rate control, Whitney (1969) proposed to use the Jacobian right pseudoinverse to obtain open-loop joint space velocity commands, which are integrated to obtain the desired joint position. However, this method may not be efficient due to unavoidable numerical drift originated by the open-loop joint velocity calculation. Another strategy to achieve operational space control goes through kinematic control (Siciliano, 1990), which consists in adding the feedback of the actual operational space position error into the resolution of the joint space velocity commands. However, these schemes have assumed that the robot is enabled with a torque controller which guarantees real-time tracking of the resulting joint space position trajectory, which is a strong assumption, since tracking may not be assured if the

control gains are mistuned and high speed desired trajectories are requested.

A stability analysis that takes into account the robot dynamics, the torque control law, and the kinematic control algorithm may provide much insight about the gain tuning and the possibility to compute a region of initial conditions where the error system solution goes to zero.

By using a Lyapunov-like analysis, the closed-loop stability of a kinematic controller used together with torque control law was studied for the first time in the work by Aicardi et al. (1995). There, this kind of robot controllers was named hierarchical control. Other formal studies on control structures based on differential kinematic algorithms published recently are found in Kelly and Moreno (2005); Vuong et al. (2009); Wang et al. (2009) and Herman (2009). Let us notice that most of these designs were focused to achieve stabilization of the error trajectory instead of assuring certain improvement of the performance of the executed trajectory.

On the other hand, frequently is found that robot actuators have a limited ability to respond to acceleration commands. Because Newton's second law, the external applied torque is proportional to the rotational acceleration, which motivates the convenience of imposing limitations in the desired acceleration to protect the actuators from large control inputs. Thus, the design of a control strategy to deal with the problem of assuring limited acceleration commands is an important topic in robot control. Particularly, the use of a control law of that kind avoids off-line replanning of the desired operational space trajectory and assures closed-loop stability.

The main aim of this paper is to introduce a new operational space trajectory tracking controller. This new scheme has the struc-

[☆] This work was supported by Secretaría de Investigación y Posgrado–IPN, and CONACyT, Mexico.

* Corresponding author.

E-mail address: moreno@citedi.mx (J. Moreno–Valenzuela).

ture of a hierarchical controller. More specifically, the proposed algorithm is defined by a model-based joint velocity controller, and a second order kinematic controller, which has the ability to produce bounded commands of joint acceleration due to the use of saturation functions. Since on-line bounded acceleration commands are produced, the new control law has the advantage of preventing possible actuator damage. A rigorous stability analysis of the closed-loop system is provided. Known theory on stability of cascaded nonlinear systems as well as standard Lyapunov's arguments are invoked. In addition to the theoretical results, the present study contributes with experimental evaluations carried out in a two degrees-of-freedom direct-drive arm. The real-time experiments show the advantage of using saturation functions in the second order kinematic controller.

This paper is organized as follows. Section 2 concern to robot dynamics and problem formulation. In Section 3, the proposed operational space controller is described, while the closed-loop stability analysis is discussed in Section 4. Experimental results are presented in section 5, and some concluding remarks are given in Section 6.

Throughout this paper the following notation will be adopted. $\lambda_{\min}\{A\}$ and $\lambda_{\max}\{A\}$ denote the minimum and maximum eigenvalues of a symmetric positive definite matrix $A \in \mathbb{R}^{n \times n}$, respectively. $\|\mathbf{x}\| = \sqrt{\mathbf{x}^T \mathbf{x}}$ stands for the norm of vector $\mathbf{x} \in \mathbb{R}^n$. $\|B\| = \sqrt{\lambda_M\{B^T B\}}$ stands for the induced norm of a matrix $B(\mathbf{x}) \in \mathbb{R}^{m \times n}$ for all $\mathbf{x} \in \mathbb{R}^n$. The notation B_r denotes the set given by the ball $\{\mathbf{x} \in \mathbb{R}^n : \|\mathbf{x}\| \leq r\}$.

2. Robot dynamics and control aim

The dynamics in joint space of a serial-chain n -link robot manipulator considering the presence of friction at the robot joints can be written as Kelly et al. (2005); Sciavicco and Siciliano (2000); Canudas et al. (1996):

$$M(\mathbf{q})\ddot{\mathbf{q}} + C(\mathbf{q}, \dot{\mathbf{q}})\dot{\mathbf{q}} + \mathbf{g}(\mathbf{q}) + F_v \dot{\mathbf{q}} + \mathbf{f}_{Cl}(\dot{\mathbf{q}}) = \boldsymbol{\tau} \quad (1)$$

where \mathbf{q} is the $n \times 1$ vector of joint displacements, $\dot{\mathbf{q}}$ is the $n \times 1$ vector of joint velocities, $\boldsymbol{\tau}$ is the $n \times 1$ vector of applied torque inputs, $M(\mathbf{q})$ is the $n \times n$ symmetric positive definite manipulator inertia matrix, $C(\mathbf{q}, \dot{\mathbf{q}})\dot{\mathbf{q}}$ is the $n \times 1$ vector of centripetal and Coriolis torques, $\mathbf{g}(\mathbf{q})$ is the $n \times 1$ vector of gravitational torques, F_v is a $n \times n$ diagonal positive definite matrix which contains the viscous friction coefficients of each joint, and $\mathbf{f}_{Cl}(\dot{\mathbf{q}})$ is a continuous and uniformly bounded function, which approaches the behavior of the Coulomb friction.

The matrix $C(\mathbf{q}, \dot{\mathbf{q}})$ —defined by using Christoffel symbols—and the time derivative of the inertia matrix $\dot{M}(\mathbf{q})$ satisfy (Kelly et al., 2005; Canudas et al., 1996):

$$\mathbf{x}^T \left[\frac{1}{2} \dot{M}(\mathbf{q}) - C(\mathbf{q}, \dot{\mathbf{q}}) \right] \mathbf{x} = 0, \quad \forall \mathbf{x}, \mathbf{q}, \dot{\mathbf{q}} \in \mathbb{R}^n. \quad (2)$$

Denoting $\mathbf{h}(\mathbf{q}) : \mathbb{R}^n \rightarrow \mathbb{R}^m$, $n \geq m$, the robot direct kinematics, where $\mathbf{q} \in \mathbb{R}^n$ is the joint positions vector, then the position and orientation $\mathbf{y} \in \mathbb{R}^m$ of the end-effector is given by:

$$\mathbf{y} = \mathbf{h}(\mathbf{q}). \quad (3)$$

The time derivative of the direct kinematic model (3) yields the differential kinematic model:

$$\dot{\mathbf{y}} = \frac{d}{dt} \mathbf{h}(\mathbf{q}) = \frac{\partial \mathbf{h}}{\partial \mathbf{q}} \dot{\mathbf{q}} = J(\mathbf{q})\dot{\mathbf{q}}, \quad (4)$$

where $J(\mathbf{q})$ is the so-called analytical Jacobian matrix (Canudas et al., 1996). The robot Jacobian describes a map from velocities in joint space to velocities in operational space.

The relationship between joint acceleration and operational space acceleration is given by the second order kinematics:

$$\ddot{\mathbf{y}} = J(\mathbf{q})\ddot{\mathbf{q}} + \dot{J}(\mathbf{q}, \dot{\mathbf{q}})\dot{\mathbf{q}}, \quad (5)$$

where $\dot{J}(\mathbf{q}, \dot{\mathbf{q}}) = (d/dt)J(\mathbf{q}) \in \mathbb{R}^{m \times n}$.

The analytical Jacobian $J(\mathbf{q})$ is assumed of full-rank ($\text{rank} = m$) and bounded by $k_j > 0$, i.e.,

$$\|J(\mathbf{q})\| \leq k_j \forall \mathbf{q} \in \mathbb{R}^n. \quad (6)$$

A useful definition in the coming analysis is:

$$J(\mathbf{q})^\dagger = J(\mathbf{q})^T [J(\mathbf{q})J(\mathbf{q})^T]^{-1},$$

which is the Jacobian right pseudoinverse (Canudas et al., 1996), assuming that $J(\mathbf{q})J(\mathbf{q})^T$ is nonsingular. Similarly, Jacobian pseudoinverse $J(\mathbf{q})^\dagger$ is assumed of full-rank ($\text{rank} = m$) and bounded by $k_j^\dagger > 0$, i.e.,

$$\|J(\mathbf{q})^\dagger\| \leq k_j^\dagger \forall \mathbf{q} \in \mathbb{R}^n. \quad (7)$$

In addition, the matrix $\dot{J}(\mathbf{q}, \dot{\mathbf{q}})$ is assumed to satisfy the relationships:

$$\dot{J}(\mathbf{q}, \mathbf{x} + \mathbf{z}) = \dot{J}(\mathbf{q}, \mathbf{x}) + \dot{J}(\mathbf{q}, \mathbf{z}), \quad \dot{J}(\mathbf{q}, \mathbf{x})\mathbf{z} = \dot{J}(\mathbf{q}, \mathbf{z})\mathbf{x}, \quad (8)$$

$$\|\dot{J}(\mathbf{q}, \mathbf{x}) - \dot{J}(\mathbf{q}, \mathbf{z})\| \leq k_{j1} \|\mathbf{x} - \mathbf{z}\|, \quad (9)$$

for all $\mathbf{x}, \mathbf{z} \in \mathbb{R}^n$. The property (9) means that the map $\dot{J}(\mathbf{q}, \dot{\mathbf{q}})$ is globally Lipschitz in $\dot{\mathbf{q}}$, uniformly in \mathbf{q} . It is possible to show that the direct kinematics a planar two degrees-of-freedom revolute joint robot satisfies assumptions (8) and (9). Therefore, these assumptions resemble properties more than assumptions.

Once the specifications are given in terms of operational space desired trajectories $\mathbf{y}_d(t)$, and under assumptions (6) and (7), the motion control problem in operational space consists in to find a control law $\boldsymbol{\tau}(t)$ so that:

$$\lim_{t \rightarrow \infty} \tilde{\mathbf{y}}(t) = \mathbf{0}, \quad (10)$$

where $\tilde{\mathbf{y}}(t) = \mathbf{y}_d(t) - \mathbf{y}(t)$ denotes the operational space position error.

Throughout this paper we assume that:

$$\|\mathbf{y}_d(t)\|, \|\dot{\mathbf{y}}_d(t)\|, \|\ddot{\mathbf{y}}_d(t)\| \leq \beta, \quad \forall t \geq 0. \quad (11)$$

Let us notice that an explicit bound on the parameter β cannot be given since it depends on the task to be executed by the robot. However, most of the desired operational space trajectories $\mathbf{y}_d(t)$ used in practice satisfy assumption (11). In fact, it is not necessary to know the precise numerical value of β ; although a computer program could be designed to approach a value.

The assumption (11) is required to show that the desired joint acceleration is bounded and to analyze the closed-loop system.

3. Proposed operational space controller

As mentioned previously, the hierarchical control structure (Aicardi et al., 1995) consists in using a primary joint velocity controller which produces the required robot torque input, and a secondary position controller that computes the joint acceleration and velocity commands for the primary loop. This Section concerns to describe the proposed hierarchical controller.

3.1. Primary loop

In order to solve the problem of operational space motion control, we first discuss the problem of joint velocity control. A model-based motion controller, like the ones addressed by Kelly et

al. (2005), to solve the motion control of robotic manipulators can be adjusted to accomplish the joint velocity control objective:

$$\lim_{t \rightarrow \infty} \tilde{\omega}(t) = 0,$$

where $\tilde{\omega}(t) = \omega_d(t) - \dot{q}(t)$ is the joint velocity error and $\omega_d(t)$ is the desired joint velocity. Such a adjustment consist in replacing the “position error” signal by the integral of the velocity error $\int_0^t \tilde{\omega}(\sigma) d\sigma$. See the paper (Moreno and Kelly, 2003) where the pure joint velocity tracking control of manipulators is studied.

In Moreno and Kelly (2003), a joint velocity controller based on the nonadaptive version of the Slotine and Li algorithm (Slotine and Li, 1991) was introduced. Based on such a results, in this paper, a new model-based joint velocity controller is introduced:

$$\tau = M(q)[\dot{\omega}_d + \gamma \tilde{\omega}] + C(q, \dot{q})[\omega_d + \gamma z] + g(q) + F_v \dot{q} + f_{cl}(\dot{q}) + K_v \tilde{\omega} + K_i z \tag{12}$$

$$\dot{z} = \tilde{\omega}, \tag{13}$$

where K_v are K_i are $n \times n$ symmetric positive definite matrices, and γ is a sufficiently small positive constant.

The controller (12)–(13) uses a constant γ instead of the matrix $\Lambda = K_v^{-1} K_i \in \mathbb{R}^{n \times n}$, as it was proposed in Moreno and Kelly (2003). Let us notice that a disadvantage of using the matrix Λ is the increasing of numerical value of the total gain associated to the velocity error $\tilde{\omega}$ and its integral z , which may eventually excite unstable modes of the robot arm. In other words, a low value of K_v may increase drastically the value of Λ . Notice also that if $\gamma = 0$, the PD+ motion control structure (Paden and Panja, 1988) is recovered.

3.2. Secondary loop

Kinematic control considers the second order kinematic model (5) as the robot model. Let us define the desired joint acceleration as:

$$\dot{\omega}_d = J(q)^\dagger [\ddot{y}_d + K_{v0} \sigma(\lambda_v \dot{\tilde{y}}) + K_{p0} \sigma(\lambda_p \tilde{y}) - \dot{J}(q, \omega_d) \omega_d], \tag{14}$$

where K_{p0} and K_{v0} are $m \times m$ symmetric positive definite matrices, ω_d is obtaining from integrating $\dot{\omega}_d$ with respect to time, and the saturation function $\sigma(\lambda_{p,v} x) = [\sigma(\lambda_{p,v} x_1), \dots, \sigma(\lambda_{p,v} x_n)]^T$ is defined by Zavala-Rio and Santibáñez (2007) as:

$$\sigma(\lambda_{p,v} x_i) = \begin{cases} l + [s - l] \tanh\left(\frac{\lambda_{p,v} x_i - l}{s - l}\right), & \text{if } \lambda_{p,v} x_i > l, \\ \lambda_{p,v} x_i, & \text{if } |\lambda_{p,v} x_i| \leq l, \\ -l + [s - l] \tanh\left(\frac{\lambda_{p,v} x_i + l}{s - l}\right), & \text{if } \lambda_{p,v} x_i < -l, \end{cases} \tag{15}$$

where $s > l > 0$, $\lambda_{p,v} > 0$, the subindexes p and v refer to the proportional and derivative parts of the kinematic controller (14),

respectively, and the desired joint velocity ω_d is obtained by integration of (14) with respect to time. The parameters s, l, λ_p and λ_v are used to modify the the slope and amplitude of the saturation function $\sigma(\lambda_{p,v} x_i)$. Therefore, we can either reinforce or attenuate the contribution of each part of the controller by selecting those parameters. The use of a more simply definition of saturation function would be possible. For example, for all $x_i \in \mathbb{R}$:

$$\sigma(\lambda_{p,v} x_i) = \tanh(\lambda_{p,v} x_i), \tag{16}$$

or:

$$\sigma(\lambda_{p,v} x_i) = \frac{\lambda_{p,v} x_i}{\sqrt{1 + [\lambda_{p,v} x_i]^2}}. \tag{17}$$

The practical assessment with real-time experiments is a way to know whether or not the use of a saturation function is convenient. As selection guideline, saturation functions with high slope at the proximity of the origin allow to reject robot model perturbations that vary slowly with time.

See Fig. 1 for a block diagram of the implementation of the proposed controller which is described by the primary joint velocity controller (12)–(13) and the secondary saturated function-based kinematic control law (14).

4. Closed-loop system analysis

By using the definition of the operational space tracking error \tilde{y} , the joint velocity error $\tilde{\omega}$, the second order kinematic model (5), property (8), and substituting the controller (12)–(13) into the robot model (1), the closed-loop system is obtained:

$$\Sigma_1 : \frac{d}{dt} \begin{bmatrix} \tilde{y} \\ \dot{\tilde{y}} \end{bmatrix} = \begin{bmatrix} \dot{\tilde{y}} \\ -K_{v0} \sigma(\lambda_v \dot{\tilde{y}}) - K_{p0} \sigma(\lambda_p \tilde{y}) \end{bmatrix} + \begin{bmatrix} 0 \\ J(q) \dot{\tilde{\omega}} + [J(q \omega_d) - \dot{J}(q, \dot{q})] \tilde{\omega} \end{bmatrix}, \tag{18}$$

$$\Sigma_2 : \frac{d}{dt} \begin{bmatrix} z \\ \tilde{\omega} \end{bmatrix} = \begin{bmatrix} \tilde{\omega} \\ -\gamma \tilde{\omega} - M(q)^{-1} [C(q, \dot{q})[\tilde{\omega} + \gamma z] + K_v \tilde{\omega} + K_i z] \end{bmatrix}. \tag{19}$$

The system (18)–(19) has a cascaded structure (Panteley and Loria, 2001) of the form:

$$\Sigma_1 : \dot{\mathbf{x}}_1 = \mathbf{f}_1(t, \mathbf{x}_1) + G(t, \mathbf{x}_1, \mathbf{x}_2) \mathbf{x}_2, \tag{20}$$

$$\Sigma_2 : \dot{\mathbf{x}}_2 = \mathbf{f}_2(t, \mathbf{x}_2), \tag{21}$$

where $\mathbf{x}_1 = [\tilde{y}^T \ \dot{\tilde{y}}^T]^T \in \mathbb{R}^{2m}$ and $\mathbf{x}_2 = [z^T \ \tilde{\omega}^T]^T \in \mathbb{R}^{2n}$. Note that the signals $[z(t)^T \ \tilde{\omega}(t)^T]^T \in \mathbb{R}^{2n}$, which come from the subsystem Σ_2

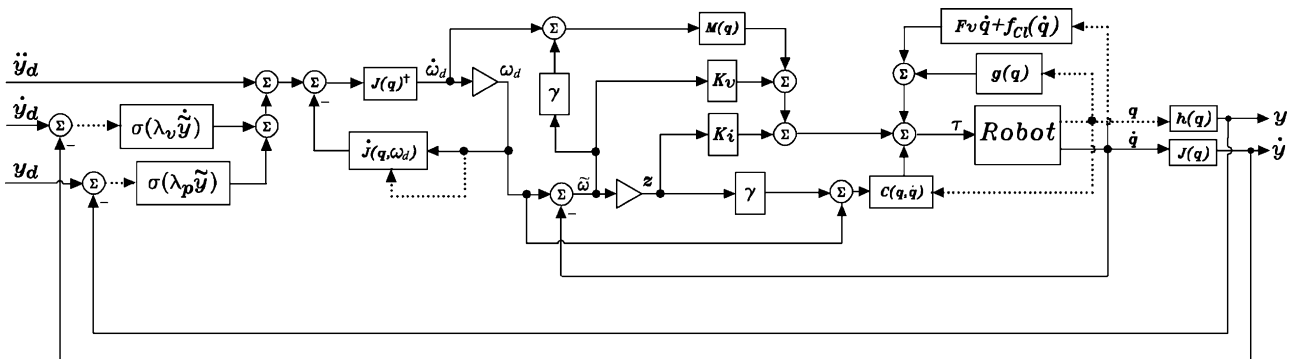


Fig. 1. Block diagram of the proposed operational space controller which is based on a primary model-based joint velocity tracking controller and a second order kinematic position controller.

in (19), perturb the subsystem Σ_1 in (18). Besides, the system (18)–(19) is a nonlinear and nonautonomous differential equation and the origin of the state space $[\tilde{\mathbf{y}}^T \dot{\tilde{\mathbf{y}}}^T \mathbf{z}^T \tilde{\omega}^T]^T = 0 \in \mathbb{R}^{2m+2n}$ is an equilibrium point.

It is worth noticing that the perturbing term in (18) can be rewritten as:

$$\begin{bmatrix} 0 & 0 \\ -J(\mathbf{q})M(\mathbf{q})^{-1}[\gamma C(\mathbf{q}, \dot{\mathbf{q}}) + K_i] & -J(\mathbf{q})[\gamma I + M(\mathbf{q})^{-1}[C(\mathbf{q}, \dot{\mathbf{q}}) + K_v]] + [j(\mathbf{q}\omega_d) - \dot{j}(\mathbf{q}, \dot{\mathbf{q}})] \end{bmatrix} \times \begin{bmatrix} \mathbf{z} \\ \tilde{\omega} \end{bmatrix},$$

which matches the notation of the perturbing term in the generalized subsystem (20).

The rest of this Section is focused in proving that the state space origin of the cascaded closed-loop system (18)–(19) is asymptotically stable and in showing that the desired joint acceleration command $\dot{\omega}_d(t) \in \mathbb{R}^n$ in (14) remains bounded for all time $t \geq 0$.

4.1. Uniform asymptotic stability

The closed-loop system (18)–(19) has the structure of nonlinear system in cascade. Comprehensive stability results for cascaded nonlinear systems have been reported by Panteley and Loria (2001). The idea is to exploit the advantage of this type of analysis, which essentially consists in verifying the uniform asymptotical stability of the subsystems Σ_1 (assuming that the perturbing term is null) and Σ_2 . Besides, the cascaded nonlinear system stability analysis requires to check a growth rate condition of the perturbing term.

In reference to the class of cascaded nonlinear systems (20)–(21) we invoke the following result.

Lemma 1. [Lemma 2 in Panteley and Loria (2001)] *If the systems:*

$$\Sigma'_1 : \dot{\mathbf{x}}_1 = \mathbf{f}_1(t, \mathbf{x}_1), \tag{22}$$

and Σ_2 in (21) are uniformly globally asymptotically stable, and the solutions of (20)–(21) are globally uniformly bounded, then (20)–(21) is uniformly globally asymptotically stable.

Proof. See Panteley and Loria (2001). \square

The following result is derived from Lemma 1.

Corollary 1. *If the system Σ'_1 in (22) and system Σ_2 in (21) are uniformly globally asymptotically stable, and the solutions of (20)–(21) are locally uniformly bounded, then (20)–(21) is uniformly locally asymptotically stable.*

Proof. The proof of Corollary 1 is obtained by following the same steps in the proof of Lemma 2 in Panteley and Loria (2001). Local arguments are used instead of the global ones. \square

To show that the closed-loop system (18)–(19) is locally uniformly asymptotically stable, the Corollary 1 is used. The proof is presented in an itemized form.

(1) The first condition is to prove the uniform global asymptotic stability of the subsystem Σ_1 with the perturbing term suppressed, that is:

$$\Sigma'_1 : \frac{d}{dt} \begin{bmatrix} \tilde{\mathbf{y}} \\ \dot{\tilde{\mathbf{y}}} \end{bmatrix} = \begin{bmatrix} \tilde{\mathbf{y}} \\ -K_{v0}\sigma(\lambda_v \dot{\tilde{\mathbf{y}}}) - K_{p0}\sigma(\lambda_p \tilde{\mathbf{y}}) \end{bmatrix}. \tag{23}$$

By using the Lyapunov function:

$$W(\tilde{\mathbf{y}}, \dot{\tilde{\mathbf{y}}}) = \sum_{i=1}^m \frac{k_{poi}}{\lambda_p} \int_0^{\tilde{y}_i} \sigma(\lambda_p x_i) dx_i + \frac{1}{2} \dot{\tilde{\mathbf{y}}}^T \dot{\tilde{\mathbf{y}}} \tag{24}$$

and Lasalle's theorem Khalil (1996), it is possible to show that $[\tilde{\mathbf{y}}^T \dot{\tilde{\mathbf{y}}}^T]^T = 0 \in \mathbb{R}^{2m}$ is a globally uniformly asymptotically stable equilibrium point of Σ'_1 in (23). Notice that Σ'_1 in (23) is a time-invariant system, whereby the uniformity is an implicit attribute of the equilibrium.

(2) The second step consists in showing that the equilibrium point of the independent system Σ_2 is globally exponentially stable. With this aim, inspired in Slotine and Li (1991), we propose the following Lyapunov function candidate:

$$V(t, \mathbf{z}, \tilde{\omega}) = \frac{1}{2} [\tilde{\omega} + \gamma \mathbf{z}]^T M(\mathbf{q}) [\tilde{\omega} + \gamma \mathbf{z}] + \frac{1}{2} \mathbf{z}^T K_i \mathbf{z}. \tag{25}$$

The time derivative of $V(\mathbf{z}, \dot{\tilde{\omega}})$ along the trajectories of the subsystem Σ_2 in (19) becomes:

$$\dot{V}(t, \mathbf{z}, \tilde{\omega}) = - \begin{bmatrix} \mathbf{z} \\ \tilde{\omega} \end{bmatrix}^T \underbrace{\begin{bmatrix} \gamma K_i & \frac{\gamma}{2} K_v \\ \frac{\gamma}{2} K_v & K_v \end{bmatrix}}_Q \begin{bmatrix} \mathbf{z} \\ \tilde{\omega} \end{bmatrix},$$

where the robot model property (2) was used. A sufficient condition for $\dot{V}(t, \mathbf{z}, \tilde{\omega})$ to be globally negative definite is that $Q > 0$. This is always fulfilled provided that γ satisfies:

$$0 < \gamma < \frac{4\lambda_{\min}\{K_i\}\lambda_{\min}\{K_v\}}{\lambda_{\max}\{K_v\}^2}.$$

Since $V(t, \mathbf{z}, \tilde{\omega})$ is a positive definite, radially unbounded and decrescent function, and $\dot{V}(t, \mathbf{z}, \tilde{\omega})$ is globally negative definite, the uniform global asymptotic stability of the equilibrium point $[\mathbf{z}^T \tilde{\omega}^T]^T = 0$ is proven (Khalil, 1996).

(3) Finally, the proof that the trajectories remain bounded for a compact set of initial conditions is given. Let us consider the Lyapunov function candidate:

$$U(t, \tilde{\mathbf{y}}, \dot{\tilde{\mathbf{y}}}, \mathbf{z}, \tilde{\omega}) = \epsilon W(\tilde{\mathbf{y}}, \dot{\tilde{\mathbf{y}}}) + V(t, \mathbf{z}, \tilde{\omega}),$$

with $\epsilon > 0$, $W(\tilde{\mathbf{y}}, \dot{\tilde{\mathbf{y}}})$ in (24) and $V(t, \mathbf{z}, \tilde{\omega})$ in (25). Notice that $U(t, \tilde{\mathbf{y}}, \dot{\tilde{\mathbf{y}}}, \mathbf{z}, \tilde{\omega})$ is a positive definite and radially unbounded function. The time derivative of $U(t, \tilde{\mathbf{y}}, \dot{\tilde{\mathbf{y}}}, \mathbf{z}, \tilde{\omega})$ along of the closed-loop system trajectories (18)–(19) is given by:

$$\begin{aligned} \dot{U}(t, \tilde{\mathbf{y}}, \dot{\tilde{\mathbf{y}}}, \mathbf{z}, \tilde{\omega}) &= -\epsilon \dot{\tilde{\mathbf{y}}}^T K_{v0} \sigma(\lambda_v \dot{\tilde{\mathbf{y}}}) \\ &\quad + \epsilon \dot{\tilde{\mathbf{y}}}^T [J(\mathbf{q})\dot{\tilde{\omega}} + [j(\mathbf{q}\omega_d) - \dot{j}(\mathbf{q}, \dot{\mathbf{q}})]\tilde{\omega}] \\ &\quad - \begin{bmatrix} \mathbf{z} \\ \tilde{\omega} \end{bmatrix}^T Q \begin{bmatrix} \mathbf{z} \\ \tilde{\omega} \end{bmatrix}. \end{aligned}$$

By using assumption (6), the fact that $\dot{\tilde{\omega}}$ is locally Lipschitz, property (9), the bounding of the desired operational space trajectories (11), the fact that there always exists a constant k_σ such that:

$$k_\sigma \|\sigma(\lambda_{p,v} \mathbf{x})\| \geq \|\mathbf{x}\|,$$

for all $\|\mathbf{x}\| \leq r$, with r arbitrarily large, and $\mathbf{x}^T \sigma(\lambda_{p,v} \mathbf{x}) \geq \|\sigma(\lambda_{p,v} \mathbf{x})\|^2$, see Zavala-Rio and Santibáñez (2007), the following inequalities hold for all $[\tilde{\mathbf{y}}^T \dot{\tilde{\mathbf{y}}}^T \mathbf{z}^T \tilde{\omega}^T]^T \in B_r \subset \mathbb{R}^{2m+2n}$:

$$-\epsilon \dot{\tilde{\mathbf{y}}}^T K_{v0} \sigma(\lambda_v \dot{\tilde{\mathbf{y}}}) \leq -\epsilon \lambda_{\min}\{K_{v0}\} \|\sigma(\lambda_v \dot{\tilde{\mathbf{y}}})\|^2, \tag{26}$$

$$\epsilon \dot{\tilde{\mathbf{y}}}^T [J(\mathbf{q})\dot{\tilde{\omega}} + [j(\mathbf{q}\omega_d) - \dot{j}(\mathbf{q}, \dot{\mathbf{q}})]\tilde{\omega}] \leq \epsilon k_\sigma c_1 \|\sigma(\lambda_v \dot{\tilde{\mathbf{y}}})\| \left\| \begin{bmatrix} \mathbf{z} \\ \tilde{\omega} \end{bmatrix} \right\|, c_1 > 0, \tag{27}$$

$$-\begin{bmatrix} \mathbf{z} \\ \dot{\tilde{\omega}} \end{bmatrix}^T Q \begin{bmatrix} \mathbf{z} \\ \dot{\tilde{\omega}} \end{bmatrix} \leq \lambda_{\min}\{Q\} \left\| \begin{bmatrix} \mathbf{z} \\ \dot{\tilde{\omega}} \end{bmatrix} \right\|^2. \quad (28)$$

By virtue of the inequalities (26)–(28), an upper bound on $\dot{U}(t, \tilde{\mathbf{y}}, \dot{\tilde{\mathbf{y}}}, \mathbf{z}, \dot{\tilde{\omega}})$ is obtained as follows:

$$\begin{aligned} \dot{U}(t, \tilde{\mathbf{y}}, \dot{\tilde{\mathbf{y}}}, \mathbf{z}, \dot{\tilde{\omega}}) \leq & - \begin{bmatrix} \|\sigma(\lambda_v \dot{\tilde{\mathbf{y}}})\| \\ \|\mathbf{z}\| \\ \|\dot{\tilde{\omega}}\| \end{bmatrix} \begin{bmatrix} \epsilon \lambda_{\min}\{K_{vo}\} & -\epsilon \frac{1}{2} k_{\sigma} c_1 \\ -\epsilon \frac{1}{2} k_{\sigma} c_1 & \lambda_{\min}\{Q\} \end{bmatrix} \\ & \times \begin{bmatrix} \|\sigma(\lambda_v \dot{\tilde{\mathbf{y}}})\| \\ \|\mathbf{z}\| \\ \|\dot{\tilde{\omega}}\| \end{bmatrix}. \end{aligned} \quad (29)$$

By Sylvester’s theorem:

$$0 < \epsilon < \frac{4\lambda_{\min}\{K_{vo}\}\lambda_{\min}\{Q\}}{k_{\sigma}^2 c_1^2} \quad (30)$$

assures that the right-hand side of inequality (29) is negative definite.

Therefore, $\dot{U}(t, \tilde{\mathbf{y}}, \dot{\tilde{\mathbf{y}}}, \mathbf{z}, \dot{\tilde{\omega}})$ is a locally negative definite function and the closed-loop is uniformly locally stable (Khalil, 1996), which implies that the closed-loop trajectories remains bounded for all initial conditions starting at some compact set $S \subset B_r$.

Since all the conditions of Corollary 1 are satisfied, we can claim:

$$\lim_{t \rightarrow \infty} \begin{bmatrix} \tilde{\mathbf{y}}(t) \\ \dot{\tilde{\mathbf{y}}}(t) \\ \mathbf{z}(t) \\ \dot{\tilde{\omega}}(t) \end{bmatrix} = 0,$$

whereby the operational space motion control objective in Eq. (10) is satisfied with the joint velocity controller (12)–(13) and the kinematic controller (14).

Notice that if the constant β in assumption (11) is numerically large, then the constant c_1 in inequality (27) should also be necessarily large. However, by inequality (30), the right-hand side of inequality (29) is negative definite irrespectively of β and c_1 . This implies that the local asymptotical stability of the state-space origin of the closed-loop system (18)–(19) is only related to the gains of the controller.

4.2. Bounding of desired joint acceleration

An important characteristic of the proposed scheme is that it is able to produce bounded commands of desired joint acceleration, which can be easily proven as shown next.

By using the triangle inequality, assumptions (7) and (11), and the property $\|\sigma(\lambda_p, v\mathbf{x})\| \leq s\sqrt{n}$, $\forall \mathbf{x} \in \mathbb{R}^n$, see Zavala-Rio and Santibáñez (2007), a upper bound on the desired joint acceleration $\dot{\omega}_d$ in (14) can be computed as follows:

$$\begin{aligned} \|\dot{\omega}_d(t)\| \leq & k_j^* \left[\beta + s\sqrt{n} \left[\lambda_{\max}\{K_{vo}\} + \lambda_{\max}\{K_{po}\} \right] \right. \\ & \left. + \sup_{\forall t \geq 0} \|\ddot{J}(\mathbf{q}(t), \omega_d(t))\omega_d(t)\| \right]. \end{aligned} \quad (31)$$

Besides, by using the definition of the joint velocity error $\tilde{\omega}$, and by triangle inequality, we have that:

$$\|\tilde{\omega}(t)\| + \|\dot{\tilde{\omega}}(t)\| \geq \|\omega_d(t)\|, \quad (32)$$

for all $t \geq 0$. Besides, using the differential map (4), and the definition of the operational space velocity error $\dot{\tilde{\mathbf{y}}}(t)$, we obtain:

$$\dot{\tilde{\mathbf{q}}} = J(\mathbf{q})^\dagger [\dot{\tilde{\mathbf{y}}}_d - \dot{\tilde{\mathbf{y}}}] \quad (33)$$

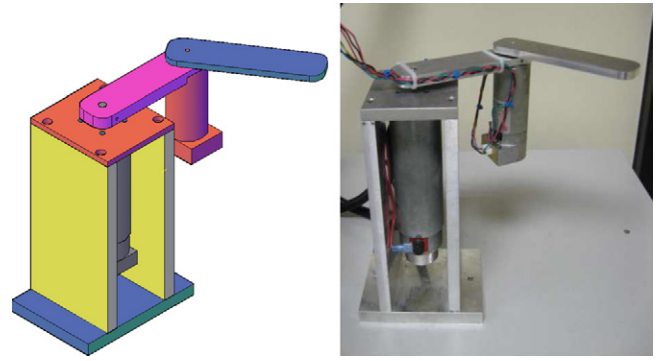


Fig. 2. Experimental robot manipulator actuated by direct-current motors.

By substituting (33) into (32), using assumptions (7) and (11), we are able to show that:

$$\|\dot{\tilde{\omega}}(t)\| + k_j^* \|\dot{\tilde{\mathbf{y}}}(t)\| + k_j^* \beta \geq \|\omega_d(t)\|, \quad \forall t \geq 0. \quad (34)$$

Because all the signals on the left-hand side of (34) are uniformly bounded, then $\omega_d(t)$ is also uniformly bounded. In consequence, the upper bound in the right-hand side of inequality (31) exists, i.e., the desired acceleration $\dot{\omega}_d(t)$ is bounded.

5. Experimental results

A planar two degrees-of-freedom direct-drive arm has been built at the CITED I – IPN Research Center. See Fig. 2 for a CAD drawing and picture. The system is composed by two DC Pittman motors operated in current mode with two Advanced Motion Controls servo amplifiers. A Sensoray 626 I/O card is used to read encoder signals with quadrature included and to transfer control commands through the D/A channels. A PC running Windows XP, Matlab, Simulink and Real-Time Windows Target is used to execute controllers in real-time with a 1 kHz sampling rate.

5.1. Practical considerations

The experimental tests are concerned with the robot pose \mathbf{y} meaning the Cartesian position of the arm tip. The direct kinematics and Jacobian are given by:

$$\begin{aligned} \mathbf{h}(\mathbf{q}) &= \begin{bmatrix} l_1 \sin(q_1) + l_2 \sin(q_1 + q_2) \\ -l_2 \cos(q_1) - l_2 \cos(q_1 + q_2) \end{bmatrix}, \\ J(\mathbf{q}) &= \begin{bmatrix} l_1 \cos(q_1) + l_2 \cos(q_1 + q_2) & l_2 \cos(q_1 + q_2) \\ l_2 \sin(q_1) + l_2 \sin(q_1 + q_2) & l_2 \sin(q_1 + q_2) \end{bmatrix}, \end{aligned}$$

where l_1 and l_2 are the link length. In the experimental robot $l_1=l_2=0.15$ [m]. The robot is actuated by direct-current motors equipped with current mode servo amplifiers. Then, the torque applied to the robot dynamics (1) is given by $\boldsymbol{\tau} = K\mathbf{u}$, where K is a 2×2 diagonal positive definite matrix, which is assumed to contain the motor constant of each DC motor actuator. The robot model can be written as:

$$K^{-1} [M(\mathbf{q})\ddot{\mathbf{q}} + C(\mathbf{q}, \dot{\mathbf{q}})\dot{\mathbf{q}} + \mathbf{g}(\mathbf{q}) + F_v \dot{\mathbf{q}} + \mathbf{f}_{cl}(\dot{\mathbf{q}})] = \mathbf{u} \quad (35)$$

Specifically, the robot model entries are as follows:

$$K^{-1}M(\mathbf{q}) = \begin{bmatrix} \theta_1 + 2\theta_2 \cos(q_2) & \theta_3 + \theta_2 \cos(q_2) \\ \theta_4 + \theta_5 \cos(q_2) & \theta_6 \end{bmatrix}, \quad (36)$$

$$K^{-1}C(\mathbf{q}, \dot{\mathbf{q}}) = \begin{bmatrix} -\theta_2 \sin(q_2)\dot{q}_2 & -\theta_2 \sin(q_2)[\dot{q}_1 + \dot{q}_2] \\ \theta_5 \sin(q_2)\dot{q}_1 & 0 \end{bmatrix}, \quad (37)$$

Table 1
Estimated parameters of the experimental robot arm; see Eqs. (36)–(39) for reference.

Parameter	Value	Unit	Parameter	Value	Unit
θ_1	0.0480	kg m V/N	θ_7	0.0070	V s/rad
θ_2	0.0037	kg m V/N	θ_8	0.0071	V s/rad
θ_3	0.0033	kg m V/N	θ_9	0.0571	V
θ_4	0.0161	kg m V/N	θ_{10}	0.0067	V
θ_5	0.0220	kg m V/N	θ_{11}	0.0554	V
θ_6	0.0162	kg m V/N	θ_{12}	0.0105	V

$$K^{-1}F_v = \text{diag}\{\theta_7, \theta_8\}, \quad (38)$$

$$K^{-1}f_{Cl}(\dot{\mathbf{q}}) = \begin{bmatrix} k_1^{-1}f_{Cl1}(\dot{q}_1) = \begin{cases} \theta_9 \tanh(50\dot{q}_1) & \text{if } \dot{q}_1 \geq 0, \\ \theta_{10} \tanh(50\dot{q}_1) & \text{if } \dot{q}_1 < 0, \end{cases} \\ k_2^{-1}f_{Cl2}(\dot{q}_2) = \begin{cases} \theta_{11} \tanh(50\dot{q}_2) & \text{if } \dot{q}_2 \geq 0, \\ \theta_{12} \tanh(50\dot{q}_2) & \text{if } \dot{q}_2 < 0, \end{cases} \end{bmatrix}. \quad (39)$$

By using the weighted least squares identification method (Gautier et al., 2001), we have estimated the coefficients involved in robot model (36)–(39), whose numerical value is shown in Table 1.

5.2. Results

By using the identified robot model (35), and the parameters in Table 1, the proposed velocity controller (12)–(13) can be implemented as:

$$\mathbf{u} = K^{-1} [M(\mathbf{q})[\dot{\omega}_d + \gamma\tilde{\omega}] + C(\mathbf{q}, \dot{\mathbf{q}})[\omega_d + \gamma\mathbf{z}] + F_v\dot{\mathbf{q}} + \mathbf{f}_{Cl}(\dot{\mathbf{q}}) + K'_v\tilde{\omega} + K'_z\mathbf{z}], \quad (40)$$

$$\dot{\mathbf{z}} = \tilde{\omega}, \quad (41)$$

where K'_v and K'_z are 2×2 positive definite matrices, whose numerical value is arbitrary.

The experimental evaluation of the proposed control scheme requires the design of an appropriate desired trajectory which gives information about the performance of the control scheme under evaluation. Periodic trajectories are well suited for that goal. The desired trajectory chosen for the experimental evaluation was:

$$\mathbf{y}_d(t) = \begin{bmatrix} y_{d1c} + r_0 \cos(\omega_0 t + \phi) \\ y_{d2c} + r_0 \sin(\omega_0 t + \phi) \end{bmatrix} [m], \quad (42)$$

with parameters $y_{d1c} = y_{d2c} = 0.1061$ [m], $\omega_0 = v_0/r_0$, $v_0 = 0.25$ [m/s], $r_0 = 0.05$ [m] and $\phi = 0.1327$ [rad]. The robot initial conditions were $\mathbf{q}(0) = [45 \ 90]^T$ [degrees].

The performance of the new kinematic controller (14) has been compared with respect to:

$$\dot{\omega}_d = J(\mathbf{q})^\dagger [\dot{\mathbf{y}}_d + K_{v0}\dot{\tilde{\mathbf{y}}} + K_{p0}\tilde{\mathbf{y}} - \dot{J}(\mathbf{q}\omega_d)\omega_d], \quad (43)$$

which does not have any saturation function in its structure. The primary joint velocity controller (12)–(13) used together with the kinematic controller with linear PD terms in (43) assure the asymptotic convergence of the position error $\tilde{\mathbf{y}}(t)$, which can be demonstrated by using a similar analysis to one showed in Section 4.

In order to keep a fair comparison scenery, the implementations of the kinematic controllers in (14) and (43) have been carried out using the proposed joint velocity controller (40)–(41). Besides, the same control gains have been used in both implementations. Specifically, for the kinematic controllers in (14) and (43) we selected:

$$K_{p0} = \text{diag}\{1.2, 2.0\} [\text{V s/rad}], \\ K_{v0} = \text{diag}\{3.0, 3.0\} [\text{V/rad}],$$

Table 2
Performance of the two controllers: settling time.

Index [s]	Linear	Saturated
T_{s,\tilde{y}_1}	13.4	1.6
T_{s,\tilde{y}_2}	10.5	1.0

while the the joint velocity controller (40)–(41) was tuned with $\gamma = 0.001$ [rad/s], and:

$$K'_i = \text{diag}\{10.0, 10.0\} [\text{V s/rad}], \\ K'_v = \text{diag}\{0.75, 0.75\} [\text{V/rad}].$$

By using the robot model in (36)–(39), with the estimated parameters in Table 1, we have compared the performance of the implemented controllers with respect to numerical simulations, where non quantized position measurements were assumed.

It is noteworthy that the simulations and experiments have been designed with the aim of showing the uniform convergence of the operational space tracking errors $[\tilde{y}_1(t)\tilde{y}_2(t)]^T$ for non zero initial conditions.

5.3. Kinematic controller with linear PD terms

The first controller tested in simulation and experiment was the primary joint velocity controller (40)–(41) and the kinematic controller with linear PD terms in (43). In Fig. 3, the trajectory tracking errors $\tilde{y}_1(t)$, $\tilde{y}_2(t)$, and the control inputs $u_1(t)$, $u_2(t)$, are shown. It is observed matching between the numerical simulation and the real-time execution of the controller. Fig. 4 shows the simulation and experimental results for the desired accelerations $\dot{\omega}_{d1}(t)$, $\dot{\omega}_{d2}(t)$, which remain bounded for all time. In addition, Fig. 4 also shows the Cartesian path $y_2(t)$ vs. $y_1(t)$ obtained experimentally, where the convergence to the circular contour is appreciated.

5.4. Kinematic controller with saturated PD terms

The results for the operational space controller described by the primary joint velocity controller (40)–(41) and the kinematic controller with saturated PD terms in (14) are described as follows. The parameters $\lambda_p = 5.0$, $\lambda_v = 1.5$, $l = 5.0$ and $s = 5.1$ were used in the saturation function (15). Figs. 5 and 6 depict the time history of the trajectory tracking errors $\tilde{y}_1(t)$, $\tilde{y}_2(t)$, the control inputs $u_1(t)$, $u_2(t)$, the desired accelerations $\dot{\omega}_{d1}(t)$, $\dot{\omega}_{d2}(t)$, and the Cartesian path $y_2(t)$ vs. $y_1(t)$. Similarly, matching of the numerical simulation and the real-time execution is appreciated.

5.5. Remarks

As predicted by theory, and corroborated in Figs. 3 and 5, the use of linear and saturated kinematic controllers guarantees the tracking of the Cartesian trajectory $\mathbf{y}_d(t)$ in (42). However, as shown in Table 2, the obtained settling times for kinematic controller with saturated PD terms are drastically smaller. The reason is that as the operational space errors $\tilde{y}_1(t)$, $\tilde{y}_2(t)$, approach to zero, the slope of the saturation functions is increased. This implies an intensification of the rate at which the time response of the system is settled. On the other hand, from Figs. 4 and 6 is observed that no important differences in the bounding of the desired acceleration $\dot{\omega}_d(t)$ are found in the two implementations, although further numerical simulations with the kinematic controller with saturated PD terms (14) showed uniform bounding of the desired acceleration for different operation conditions. Another important observation is the high frequency oscillations in the time history of the control inputs $u_1(t)$, $u_2(t)$. A previous simulation study showed that those oscillations are occasioned by the quantized measurement of the

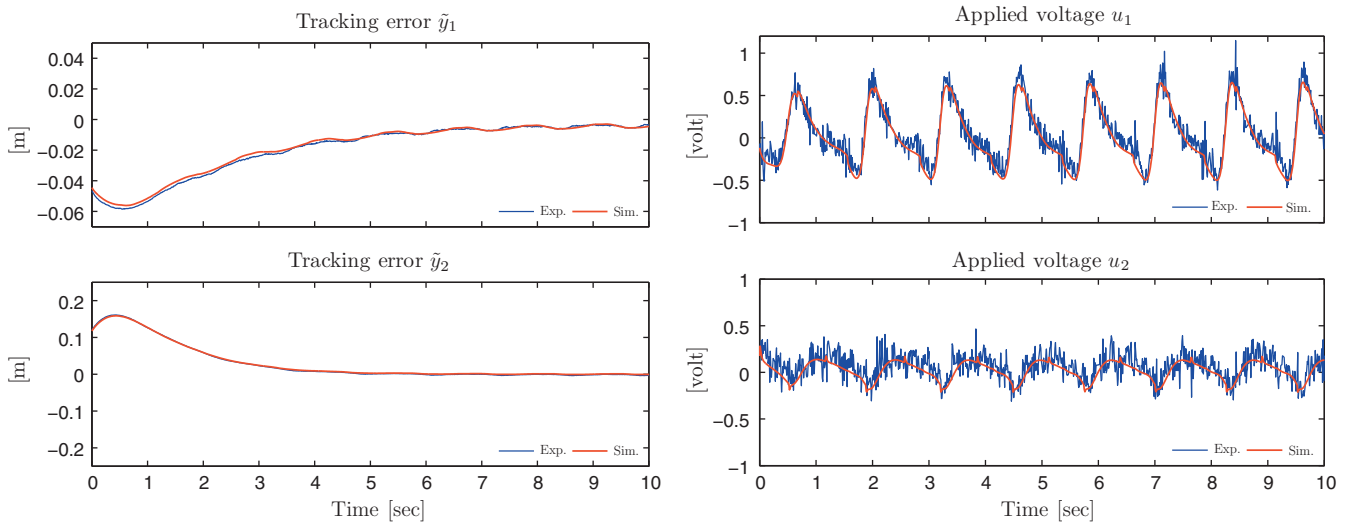


Fig. 3. Kinematic controller with linear PD terms: simulation and experiment of the time histories of the tracking errors $\tilde{y}_1(t)$ and $\tilde{y}_2(t)$, and the control input $u_1(t)$ and $u_2(t)$.

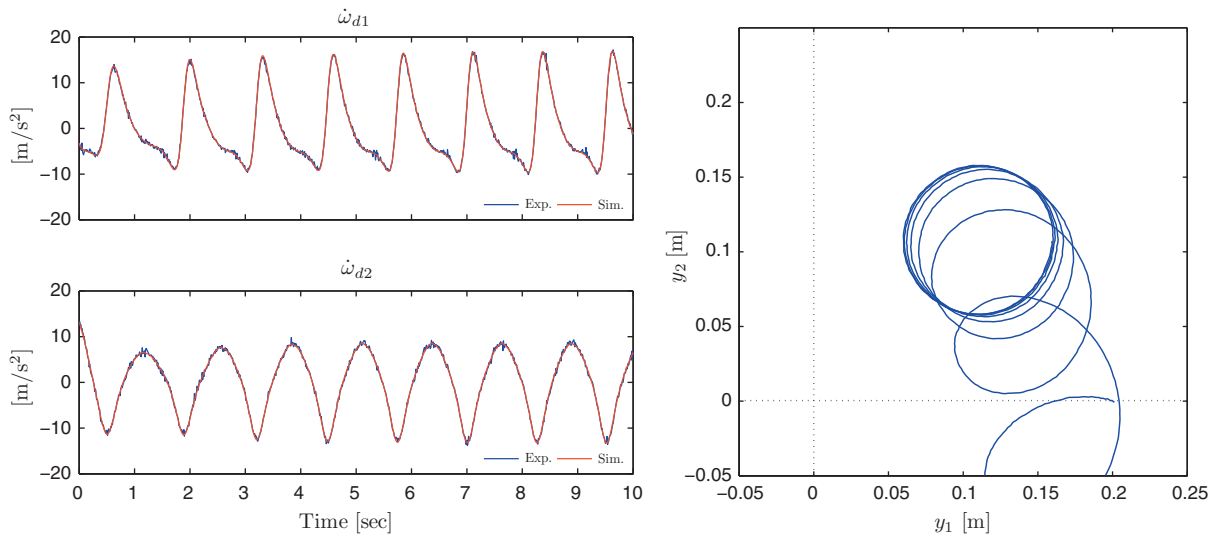


Fig. 4. Kinematic controller with linear PD terms: simulation and experiment of the time histories of the desired acceleration $\dot{\omega}_{d1}(t)$ and $\dot{\omega}_{d2}(t)$, and experimental result of $y_2(t)$ vs $y_1(t)$.

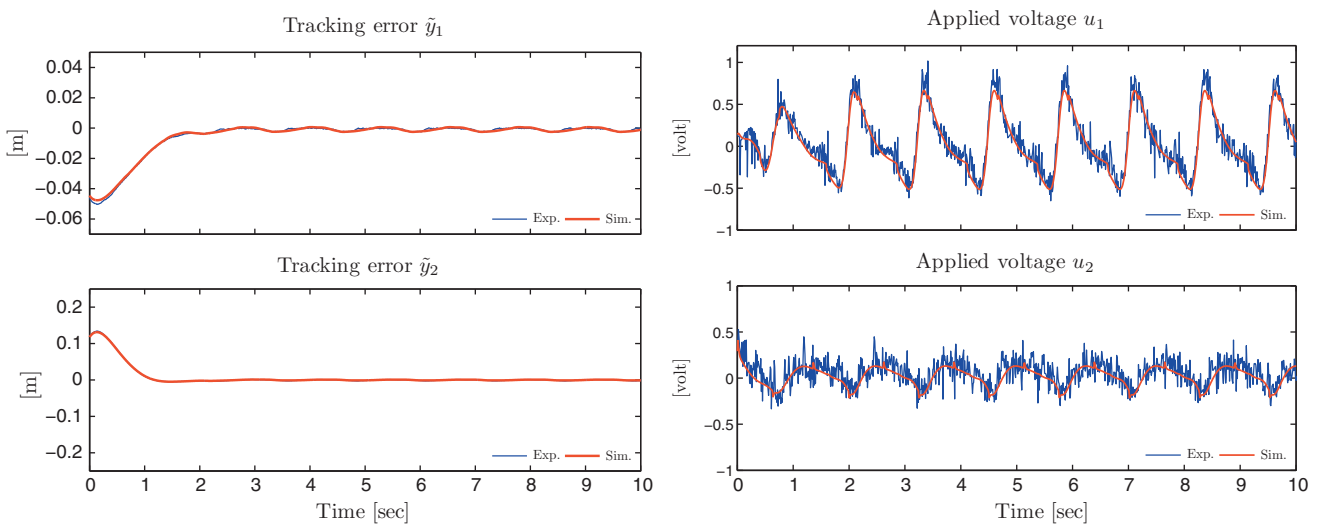


Fig. 5. Kinematic controller with saturated PD terms: simulation and experiment of the time histories of the tracking errors $\tilde{y}_1(t)$ and $\tilde{y}_2(t)$, and the control input $u_1(t)$ and $u_2(t)$.

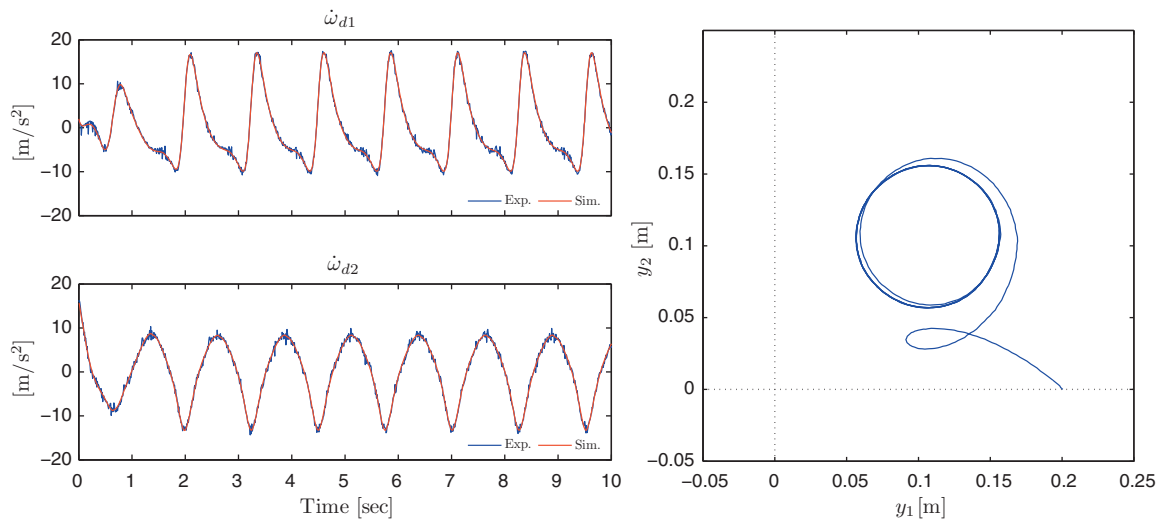


Fig. 6. Kinematic controller with saturated PD terms: simulation and experiment of the time histories of the desired acceleration $\dot{\omega}_{d1}(t)$ and $\dot{\omega}_{d2}$, and experimental result of $y_2(t)$ vs. $y_1(t)$.

joint position, velocity estimation via Euler approximation and the discrete implementation at 1 kHz of sampling rate.

6. Summary

A feedback structure composed by a primary joint velocity controller and a kinematic controller with saturated PD terms was introduced. The new scheme achieves motion control in the operational space of the robot manipulator. By using stability theory of cascaded nonlinear systems, the uniform asymptotical stability of the closed-loop system was proven in a rigorous way. Our study included experimental evaluations, where the ability of the new controller to draw a circular contour in the Cartesian space of a two degrees-of-freedom robot was verified.

References

- Aicardi, M., Caiti, A., Cannata, G., Casalino, G., 1995. Stability and robustness of a two layered hierarchical architecture for the closed loop control of robots in the operational space. In: in Proc. of the IEEE International Conference on Robotics and Automation, Nagoya, Japan, pp. 2771–2778.
- Canudas, C., Siciliano, B., Bastin, G. (Eds.), 1996. Theory of Robot Control. Springer-Verlag, London.
- Gautier, M., Poignet, Ph., 2001. Extended Kalman filtering and weighted least squares dynamic identification of robot. Control Engineering Practice 9 (12), 1361–1372.
- Herman, P., 2009. A quasi-velocity-based nonlinear controller for rigid manipulators. Mechanics Research Communications 36 (7), 859–866.
- Kelly, R., Santibáñez, V., Loria, A., 2005. Control of Robot Manipulators in Joint Space. Springer-Verlag, London.
- Kelly, R., Moreno, J., 2005. Manipulator motion control in operational space using joint velocity inner loops. Automatica 41 (8), 1423–1432.
- Khalil, H., 1996. Nonlinear Systems. Prentice-Hall, Upper Saddle River.
- Moreno, J., Kelly, R., 2003. Velocity control of robot manipulators: analysis and experiments. International Journal of Control 76 (14), 1420–1427.
- Paden, B., Panja, R., 1988. Globally asymptotically stable PD+ controller for robot manipulators. International Journal of Control 7 (6), 1697–1712.
- Panteley, E., Loria, A., 2001. Growth rate conditions for uniform asymptotic stability of cascaded time-varying systems. Automatica 37 (3), 453–460.
- Sciavicco, L., Siciliano, B., 2000. Modeling and Control of Robot Manipulators. Springer, London.
- Siciliano, B., 1990. Kinematic control of redundant robot manipulators: a tutorial. Journal of Intelligent and Robotic Systems 3, 201–212.
- Slotine, J.J., Li, W., 1991. Applied Nonlinear Control. Englewood Cliffs, Prentice-Hall.
- Vuong, N.D., Ang, M.H., Lim, T.M., Lim, S.Y., 2009. Multi-rate operational space control of compliant motion in robotic manipulators. In: In Proc. of the 2009 IEEE International Conference on Systems, Man and Cybernetics, San Antonio, TX, pp. 3175–3180.
- Wang, L., Chai, T., Fang, Z., 2009. Neural-network-based two-loop control of robotic manipulators including actuator dynamics in task space. Journal of Control Theory and Applications 7 (2), 112–118.
- D.E. Whitney, Resolved motion rate control of manipulators and human prostheses, IEEE Transactions on Man-Machine Systems, vol. MMS-10, no. 2, 47–53, 1969.
- Zavala-Rio, A., Santibáñez, V., 2007. A natural saturating extension of the PD-with-gravity-compensation control law for robot manipulators with bounded inputs. IEEE Transactions on Robotics 23 (2), 386–391.